Supplementary Information

Sulfur doping activated metal-support interaction drives Pt nanoparticles to achieve acid-base hydrogen evolution reaction

Yagang Li, [b] Jiaqing Luo, [*c] Peilin Liu, [b] Liangkun Zhang, [b] Weiyu Song, [a,b] Yuechang Wei, [a,b] Zhen Zhao, [a,d] Xiao Zhang, [*a,b] Jian Liu [a,c] and Yuanqing Sun [*a,b]

a. State Key Laboratory of Heavy Oil Processing, China University of Petroleum, Beijing 102249, China

b. College of Science, Beijing Key Lab of Oil & Gas Optical Detection Technology, and Basic Research Center for Energy Interdisciplinary, China University of Petroleum, Beijing 102249, China

c. State Key Laboratory of Heavy Oil Processing at Karamay, China University of Petroleum Beijing at Karamay, Karamay 834000, China

d. Institute of Catalysis for Energy and Environment, College of Chemistry and Chemical Engineering, Shenyang Normal University, Shenyang, 110034, China

*Corresponding Author,

E-mail: yqsun@cup.edu.cn; luojiaqing@cupk.edu.cn; zhangxiao@cup.edu.cn.

DFT Theoretical Calculation Supplementary Note

1. Design and optimization of the calculated catalyst model

The model employed in the theoretical calculations was designed based on the experimental observations. In our models, Pt NPs on NSC and NC support are represented by an octahedron with fcc structure composed of 13 metal atoms. In turn, the substrate is represented by the 5 x 5 supercell of (110) surface of a graphene. In this model, nitrogen and sulfur doping is achieved by substituting carbon atoms in the lattice. The three nitrogen atoms and one sulfur atom to distinct of primary and secondary dopants in the simulation process. All of the periodic models of density-functional theory (DFT) in this work were calculated with the Vienna ab initio simulation package (VASP) code.[1] the Grimme method (DFT-D3) was incorporated to take into account the weak van der Waals interactions.[2] The projected augmented wave (PAW) method in real space was utilized to solve the single electron wavefunction at the ground state, with a cut-off energy of 500 eV for the plane wave basis set.[3] All structures were fully relaxed and optimization was considered convergent when the maximum force was below 0.05 eV $Å^{-1}$ and the convergence criterion of self-consistency reached 10^{-5} eV.[4] In order to simulate the reaction mechanism of electrolytic water hydrogen evolution, some small molecules (H_2O, H, H_2) be adsorbed at the active site on the edge of Pt nanoparticles to form the corresponding adsorption state structure (Fig. S25 and Fig. S26).

2. The binding energy

The binding energy was utilized as a parameter to assess the thermodynamic stability of Pt nanoparticle adsorption on the substrate surface with various interface modifications. The binding energy between nanoparticle and graphene was calculated as follows：

$$\Delta E_{Binding} = E_{total} - E_{nanoparticle} - E_{graphene}$$

Where E_{total} represents the total energy of the optimized adsorption system, $E_{nanoparticle}$ denotes the energy of the isolated adsorbate and $E_{graphene}$ signifies the energy of the catalytic material's substrate.

The binding energy serves as an indicator of the strength of interaction between the adsorbent and the substrate. A positive binding energy signifies lower thermodynamic stability within the adsorption system, indicating weaker interactions that are less favorable for binding. Conversely, a negative value

denotes higher thermodynamic stability, suggesting stronger interactions and more favorable conditions for the adsorption process.[5,6]

3. Differential Charge Density

Differential charge density is widely recognized as a fundamental concept in quantum chemistry and solid-state physics, describing the variations in electron density during specific physical processes or chemical reactions. Differential charge density represents the difference between the charge density of a bonded system and the sum of the individual atomic charge densities prior to bonding.

Differential Charge Density of AB system is obtained as follows.

$$\Delta\rho = \rho_{AB} - \rho_A - \rho_B$$

The charge densities of the AB, A, and B systems are calculated separately in VASP. It is worth noting that the status and position of A and B should be consistent with those of AB.[7]

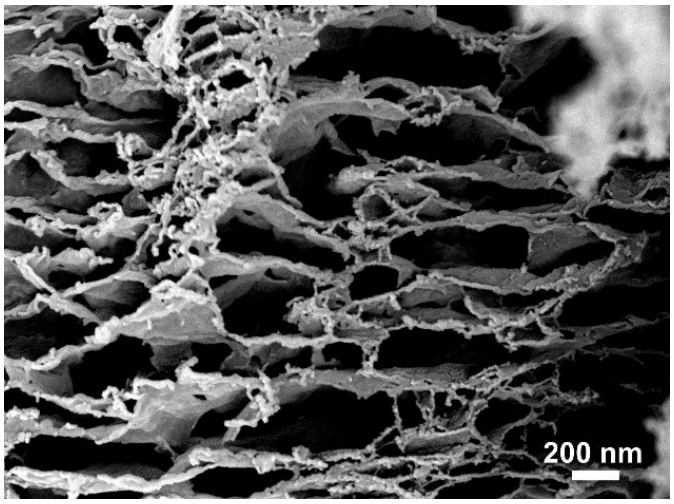

Fig. S1 SEM image of Pt/NC

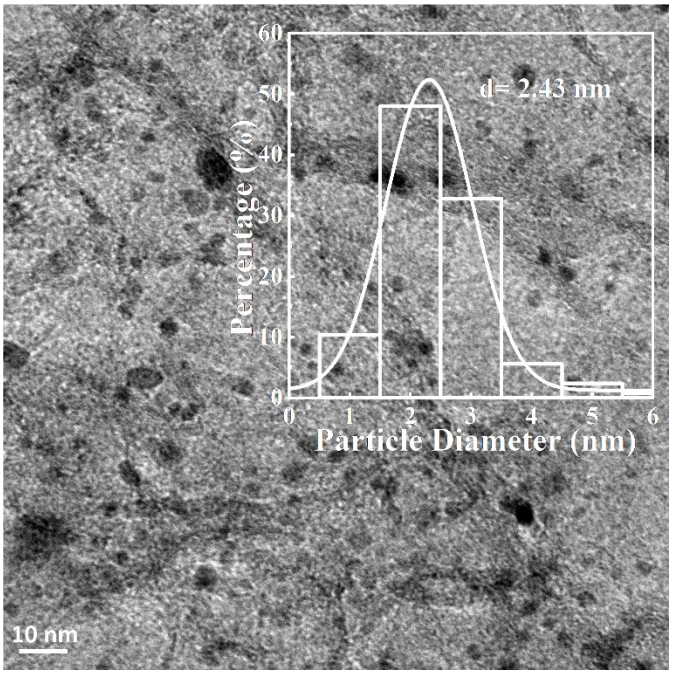

Fig. S2 TEM image of Pt/NC (inset: particle size-distribution of Pt NPs).

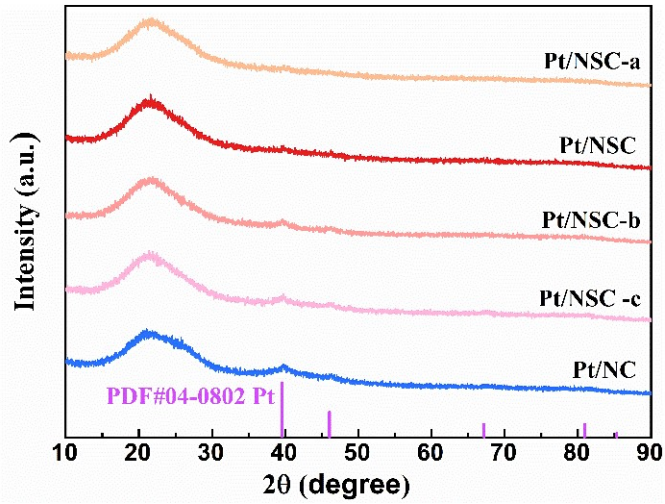

Fig. S3 XRD patterns of Pt/NSC, Pt/NC and Pt/NSC-x (x = a, b, c).

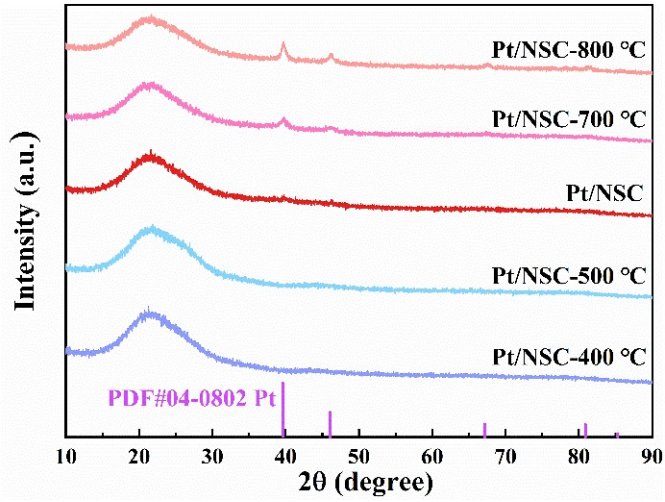

Fig. S4 XRD of Pt/NSC and Pt/NSC-x (400, 500, 700, 800℃).

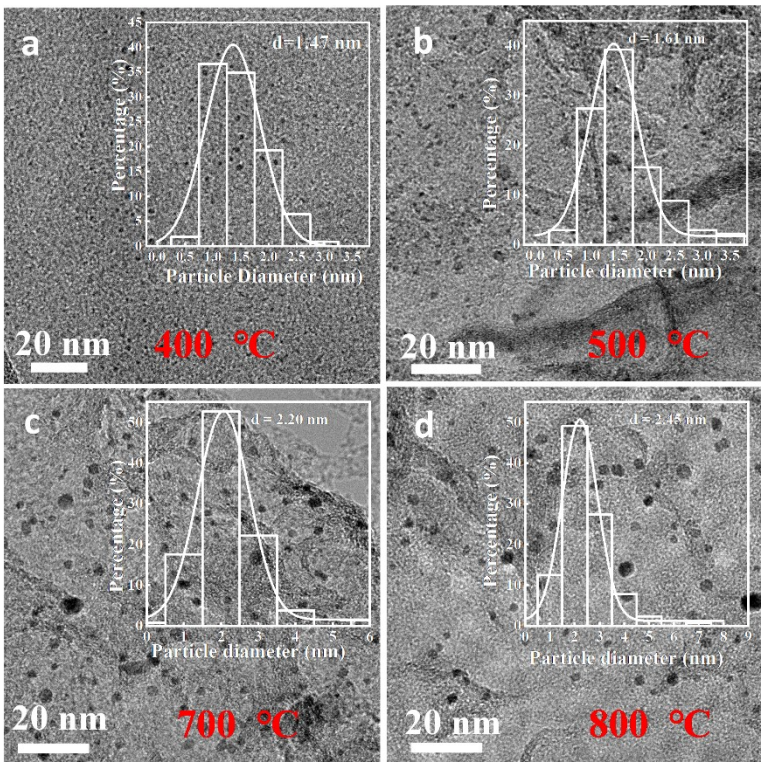

Fig.S5 TEM images of Pt/NSC (a) 400 °C, (b) 500 °C, (c) 700 °C, (b) 800 °C and corresponding particle size distribution histograms.

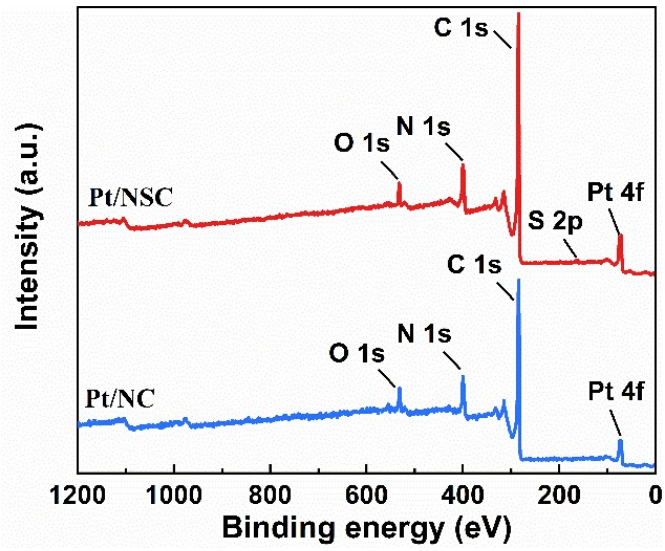

Fig. **S6** The XPS spectra of Pt/NSC and Pt/NC.

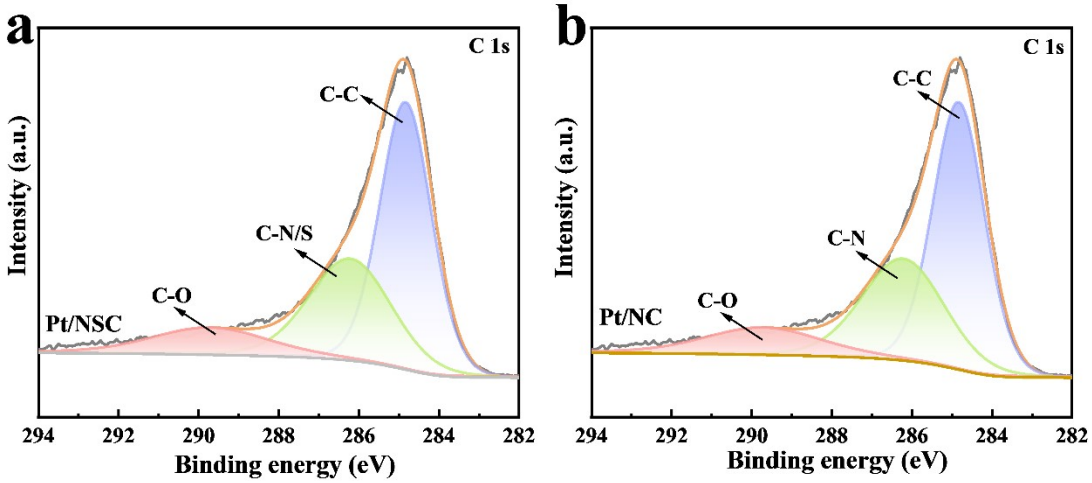

Fig. **S7** C 1s of XPS spectra of Pt/NSC (a) and Pt/NC (b).

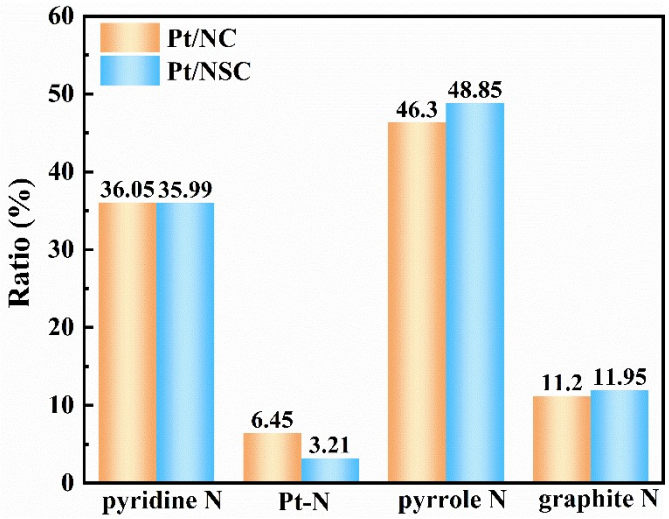

Fig.S8 Comparison of different N types of Pt/NSC and Pt/NC.

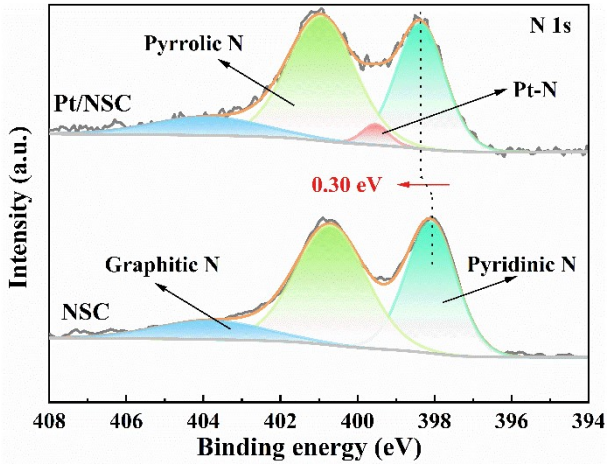

Fig. S9 N 1s XPS spectra of Pt/NSC and NSC.

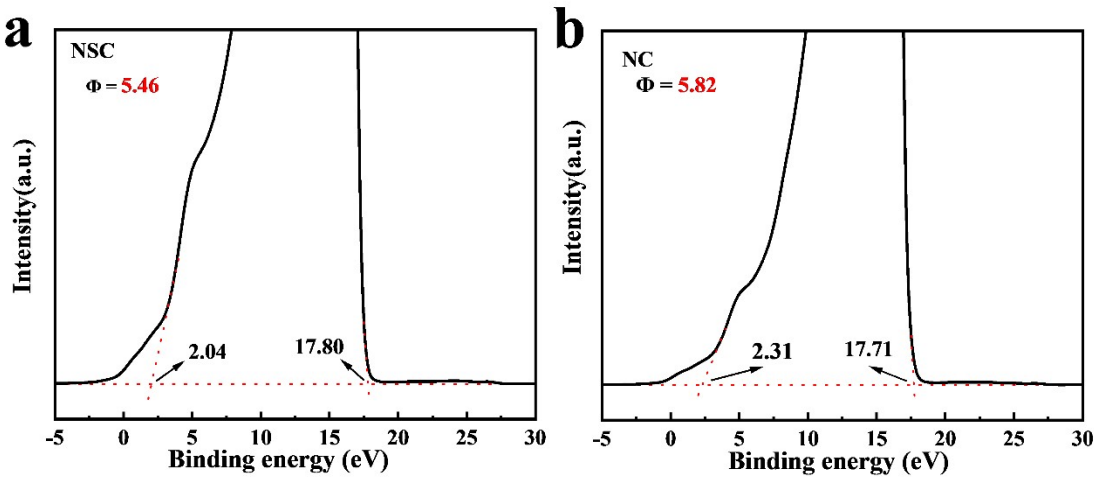

Fig. S10 The $E_{cut\text{-}off}$ and E_f of NSC (a) and NC (b) by UPS test, the work function according to the formula: $W_f = 21.22\ eV + E_{cut\text{-}off} - E_f$.

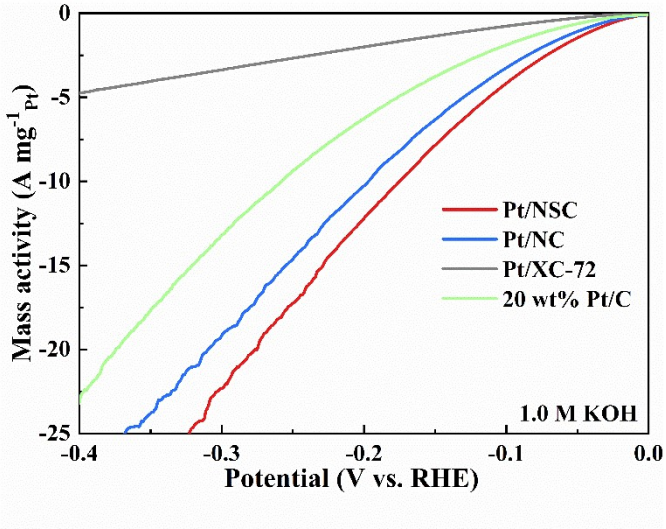

Fig. S11 The mass activity of Pt/NSC, Pt/NC, 20 wt% Pt/C, Pt/XC-72, and NSC in 1.0 M KOH.

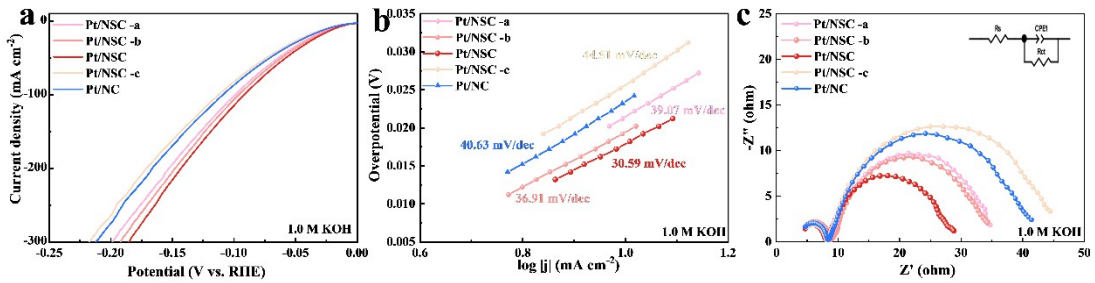

Fig. S12 The Electrocatalytic HER performance of Pt/NSC, Pt/NC and Pt/NSC-x (x = a, b, c) in 1.0 M KOH. (a) Polarization curves. (b) Tafel plots, (c) Nyquist plots.

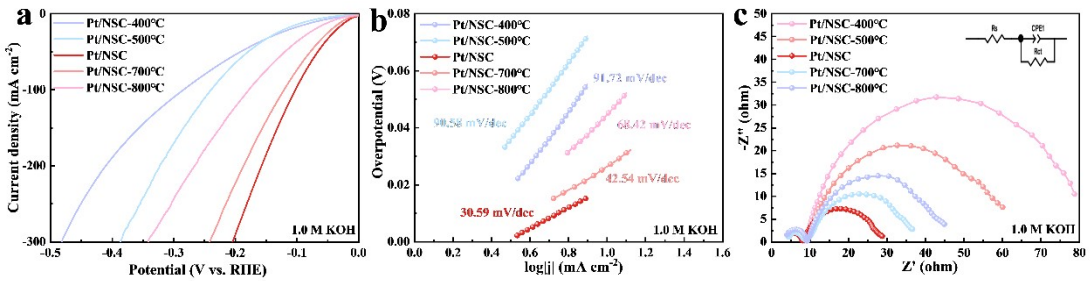

Fig. S13 The HER performance of Pt/NSC and Pt/NSC-x (x = 400, 500, 700, 800℃) in 1.0 M KOH. (a) Polarization curves. (b) Tafel plots, (c) Nyquist plots.

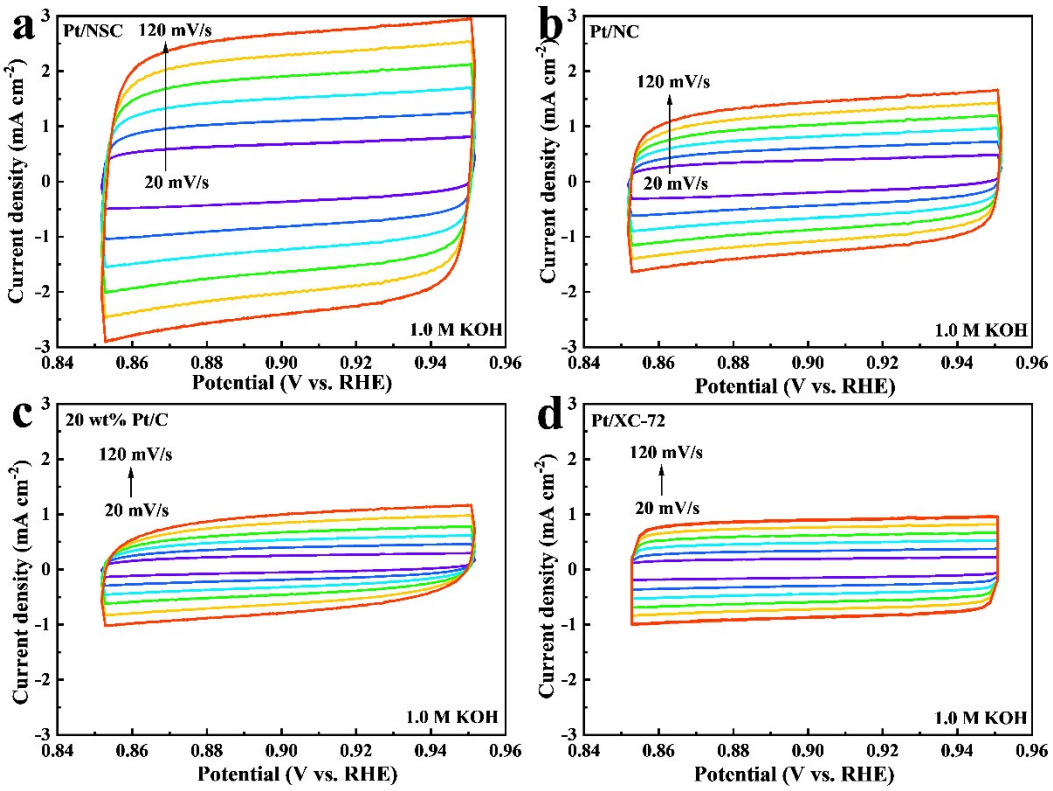

Fig. S14.CV curves in the non-Faradaic region of all samples with scan rates of 20, 40, 60, 80, 100, and 120 mV s^{-1}, respectively.

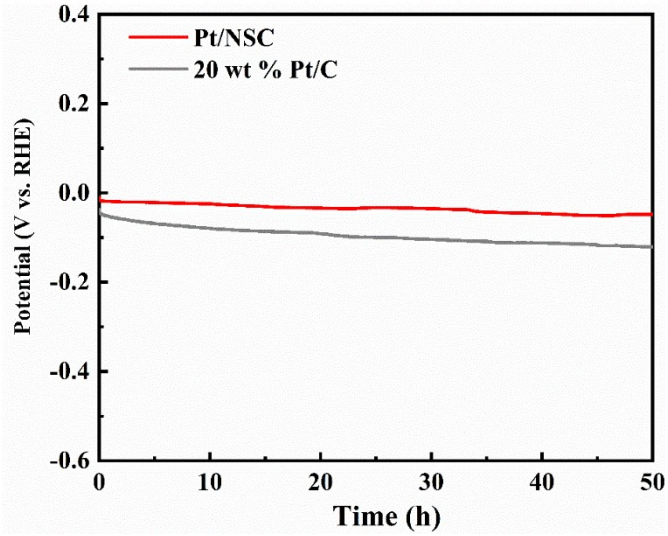

Fig. S15 chronopotentiometry tests of Pt/NSC and 20 wt % Pt/C for 50 h at 10 mA cm^{-2} in 1.0 M KOH.

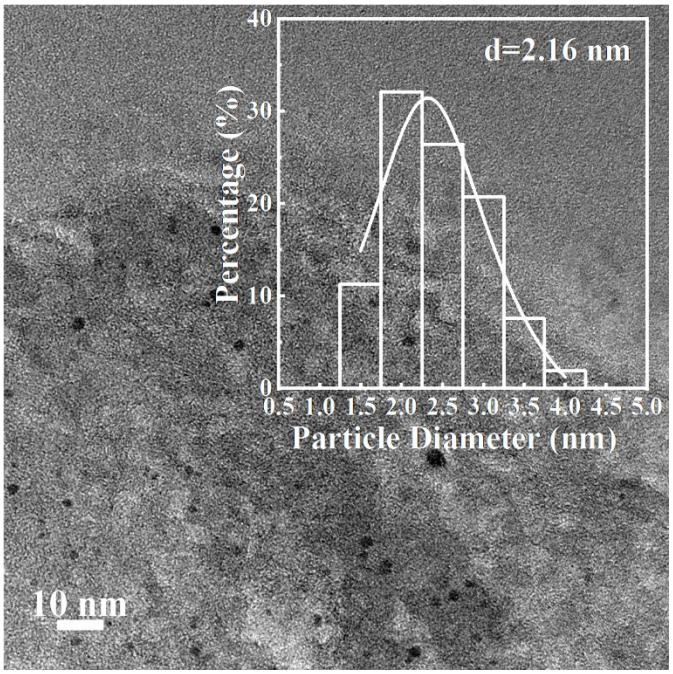

Fig.S16 HR-TEM image of Pt/NSC after the chronopotentiometry test at 50 mA cm^{-2} in 1.0 M KOH (inset: size-distribution histogram of Pt NPs).

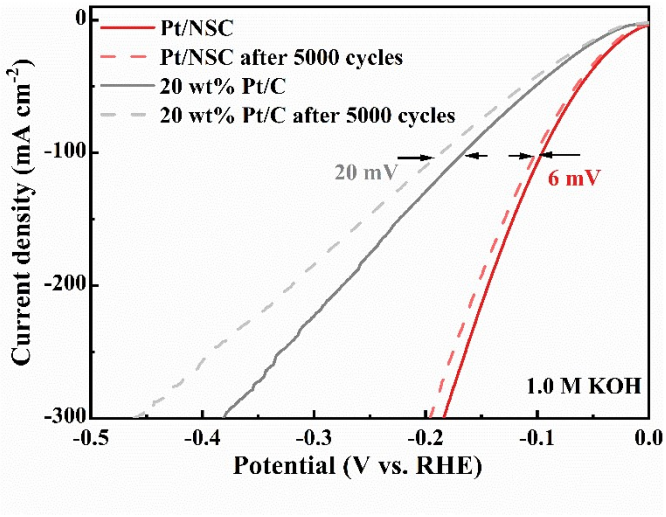

Fig.S17 Comparing the LSV curves after 5000 CV cycles of the Pt/NSC and 20 wt% Pt/C in 1.0 M KOH.

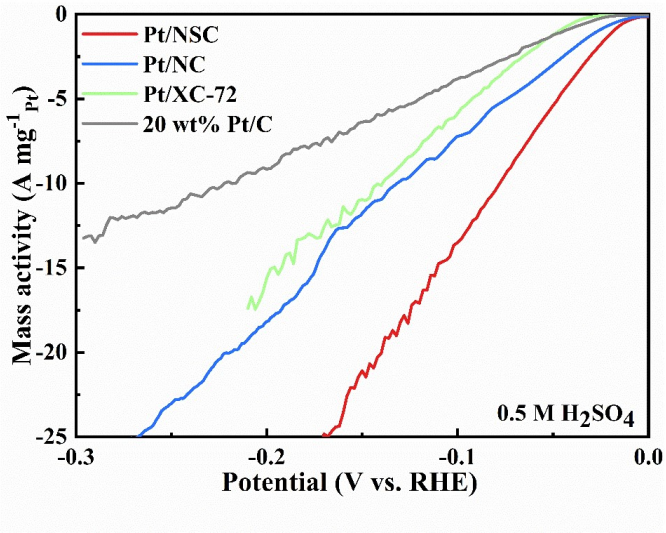

Fig. S18 The mass activity of Pt/NSC, Pt/NC, 20 wt% Pt/C, Pt/XC-72, and NSC in 0.5 M H_2SO_4.

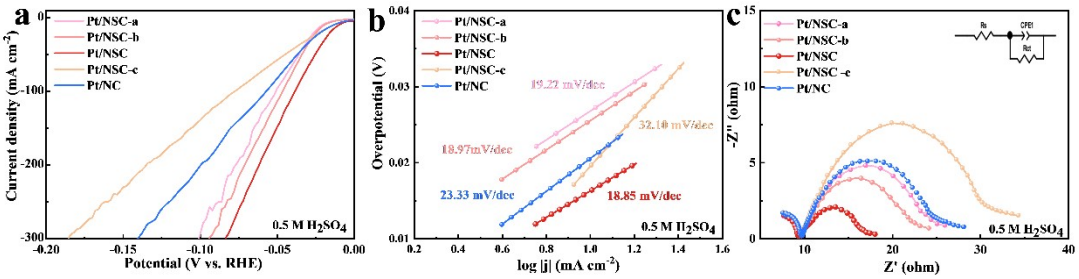

Fig.**S19** The Electrocatalytic HER performance of Pt/NSC, Pt/NC and Pt/NSC-x (x = a, b, c) in 0.5 M H_2SO_4. (a) Polarization curves. (b) Tafel plots, (c) Nyquist plots.

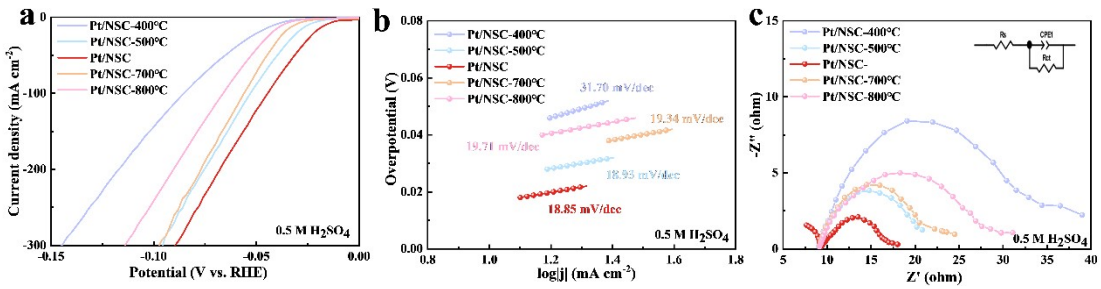

Fig.S20 The HER performance of Pt/NSC and Pt/NSC-x (x=400, 500, 700, 800 ℃) in 0.5 M H_2SO_4. (a) Polarization curves. (b) Tafel plots, (c) Nyquist plots.

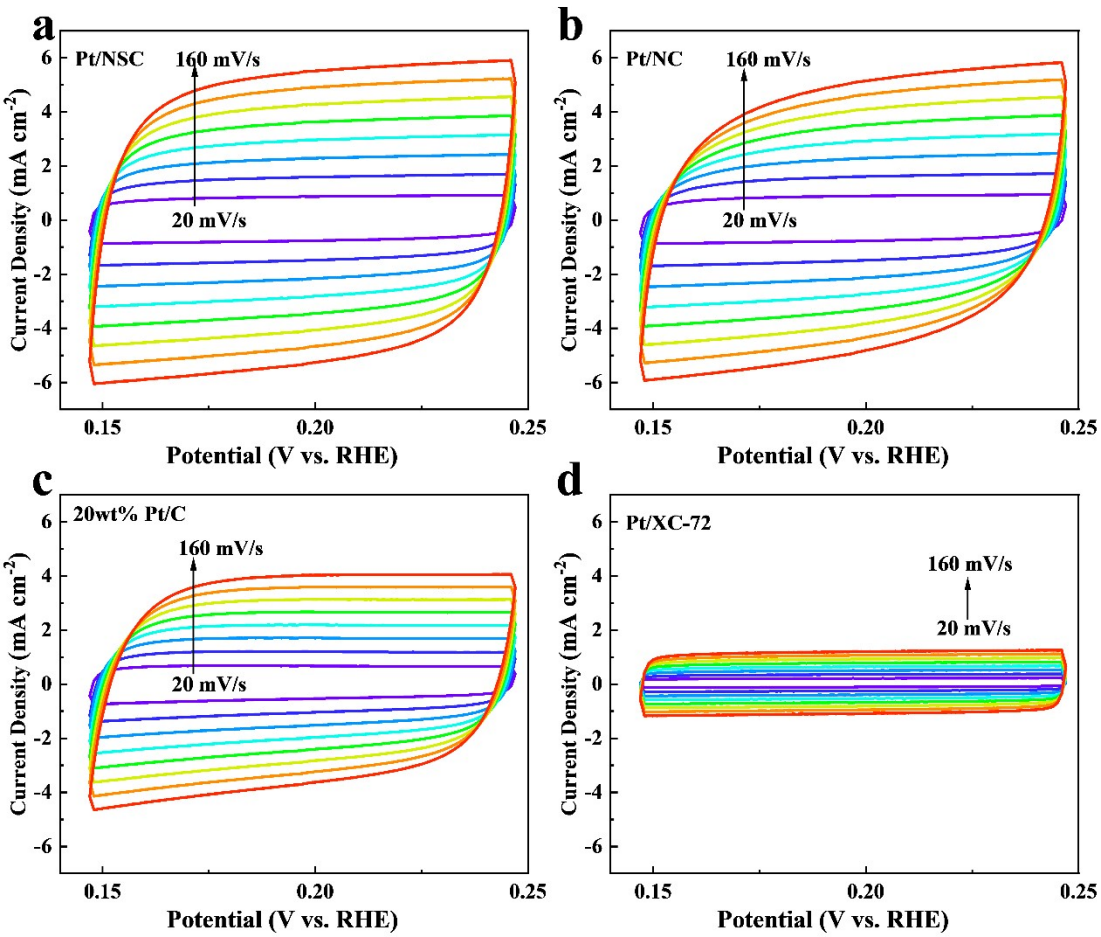

Fig. S21 CV curves in the non-Faradaic region of all samples with scan rates of 20,40, 60, 80, 100, and 120 mV s^{-1}, respectively.

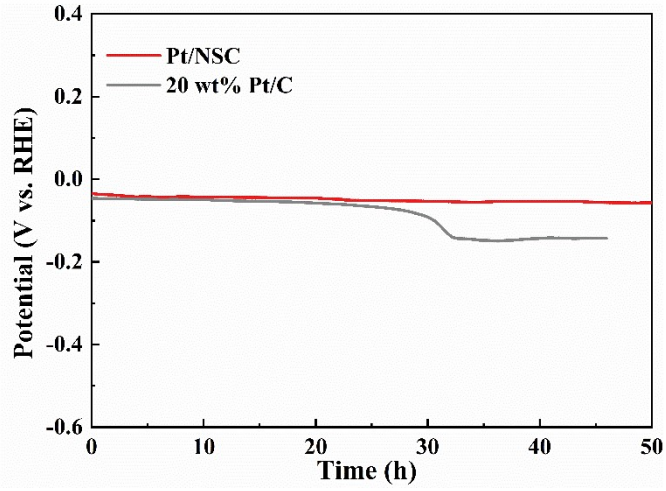

Fig. S22 Chronopotentiometry tests of Pt/NSC and 20 wt % Pt/C for 50 h at 10 mA cm^{-2} in 0.5 M H_2SO_4.

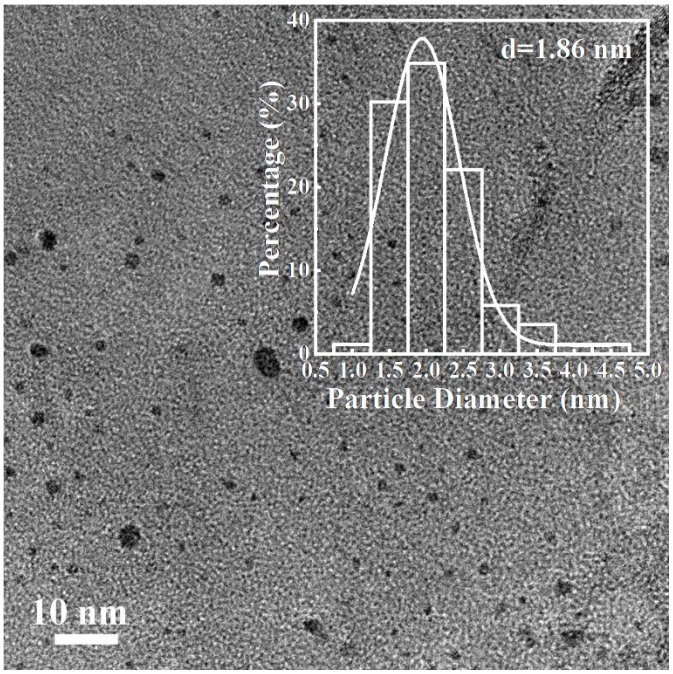

Fig. S23 HR-TEM image of Pt/NSC after the chronopotentiometry test at 50 mA cm^{-2} in 0.5 M H_2SO_4 (inset: size-distribution histogram of Pt NPs).

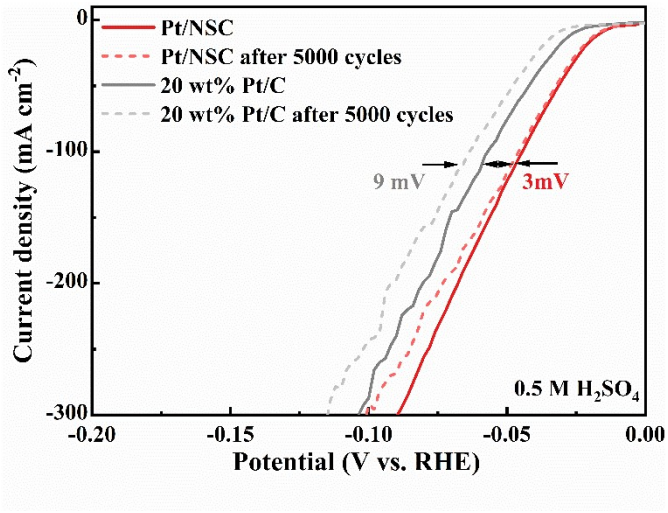

Fig.S24 Comparing the LSV curves after 5000 CV cycles of the Pt/NSC and 20 wt% Pt/C in 0.5 M H_2SO_4.

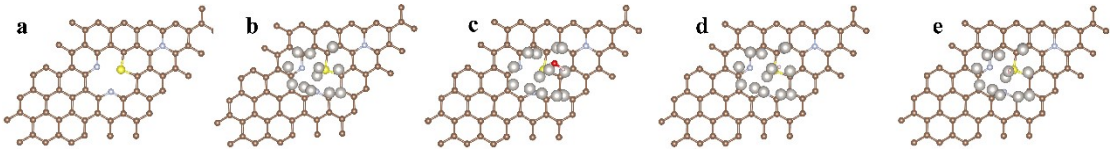

Fig. S25 Model diagrams of Pt / NSC. (a) NSC, Nitrogen and sulfur doping are achieved by substituting carbon atoms in the lattice, and the number of heteroatomic doping is used to distinguish between primary and secondary doping. (b) Pt/NSC, Pt NPs on NSC support are represented by an octahedron composed of 13 metal atoms. Small molecules (H_2O, H, H_2) be adsorbed at the active site on the edge of Pt nanoparticles to simulate the corresponding adsorption state structure. (c) H_2O*Pt/NSC. (d) H*Pt/NSC, (e) H_2*Pt/NSC.

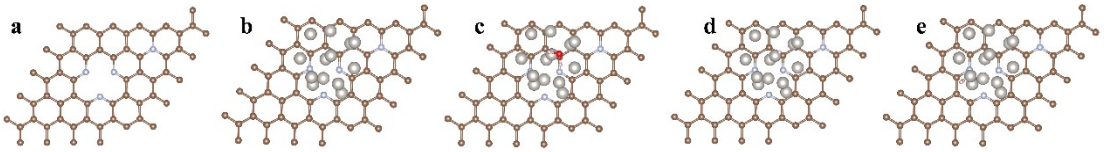

Fig. S26 Model diagrams of Pt / NC. (a) NC, Nitrogen doping is achieved by substituting carbon atoms in the lattice. (b) Pt/NC, Pt NPs on NC support are represented by an octahedron composed of 13 metal atoms. Small molecules (H_2O, H, H_2) be adsorbed at the active site on the edge of Pt nanoparticles to simulate the corresponding adsorption state structure. (c) H_2O*Pt/NC. (d) H*Pt/NC, (e) H_2*Pt/NC.

Table S1 Quantitative analysis of ICP-MS elements in Pt/NSC

Test element	Percentage content （wt %）
S	**0.28**
Pt	**7.677**

Table S2 Comparison of alkaline media properties of Pt-based catalysts

Catalyst	Overpotential (mV) @10 mA cm^{-2}	Tafel slope (mV dec^{-1})	journal
Pt/NSC	17.8	30.59	This work
Pt/C	32.9	46.21	This work
$Au@Pt_{1.5}Co_{0.08}$	14	29	J. Energy Chem, 2022, 69, 44–53
d-Pt−Ni	15	29	ACS Mater. Lett, 2021, 3, 1738−1745
Pt/8-NCNT	17	33.3	Adv. Energy Mater, 2022, 12, 2200110
$Pt/CeO_x/C$ (3nm)	19	50	Adv. Funct. Mater, 2024, 2402966
Pt-AC/Cr−N−C	19	30	J. Am. Chem. Soc, 2023, 145, 21432–21441
$Pt_{0.5}Fe_{0.5}@CNOs$	19	23.9	Appl. Surf. Sci, 2023, 636, 157860
Pt-30/NCM	19.5	40.8	Chem. Eng. J, 2022,436, 135186
Pt/FeOOH@NiFe LDHs	20	51	ACS. Catal, 2024, 14, 7867−7876
Pt_{SA}-Pt_C/NDPCM	20	58.9	Adv. Funct. Mater, 2023, 2304852
MXene/B-Pt	20	51.8	J. Mater. Chem. A, 2023, 11, 5830–5840
$Pt_{61}Ga_{39}$ @CNT	20	31.7	App. Catal. B-environ, 2023, 322, 122100
$Pt_{SAC}–N_xC_y$	24	60.25	ACS Appl. Mater. Interfaces, 2023, 15, 29195-29203
PANI@Pt/S-TiN NTs/Ti	12	31.2	Small, 2022, 18, 2205603
PtC_{60}	24.3	41.9	Nat. Commun, 2023, 14:1711
Pt/C_{60}-2/KB	25	55	Nat. Commun, 2023, 14:2460
Pt_3Fe/NMCS-A	29	50	Adv. Mater, 2023, 35, 2303030
CoPt-Pt_{SA}/NDPCF	31	43.65	Adv. Funct. Mater, 2022, 32, 2205920
Pt_3Co@NCNT	36	34.8	Angew. Chem. Int. Ed, 2021, 60, 19068–19073
PtNi-NC-900	37.4	43.2	J. Mater. Chem. A, 2022, 10, 13727–13734
PtM@CN-HF	38	69.5	Chem. Eng. J, 2024, 481, 148430
$Pt_1Ru_x@C$	48.7	55.6	J. Mater. Chem. A, 2024, 12, 4108–4122
$Pd_7@Pt_3$	49	42.7	Mater. Horiz, 2024, 11, 1964
$PtRu/CNT@SnO_{2-x}$	53	48	J. Am. Chem. Soc, 2024, 146, 21453−21465

Table S3 Comparison of acidic media properties of Pt-based catalysts

Catalyst	Overpotential (mV) @10 mA cm^{-2}	Tafel slope (mV dec^{-1})	journal
Pt/NSC	10.2	18.85	This work
Pt/C	21.1	20.18	This work
Pt@NCL-CNF	5.3	30.9	Int. J. Hydrogen. Energy, 2024, 71, 1242–1254
PtM@CN-HF	6	33	Chem. Eng. J, 2024, 481, 148430
$Pt_{0.5}Fe_{0.5}$@CNOs	11	12.5	Appl. Surf. Sci, 2023, 636, 157860
5% 1T-PtO_2/C	12	18.6	Energy Environ. Sci, 2023, 16, 574–583
PANI@Pt/S-TiN NTs/Ti	12	26.9	Small, 2022, 18, 2205603
Pt_3Fe/NMCS-A	13	21	Adv. Mater, 2023, 35, 2303030
Pt_1Ru_x@C	13.15	20.7	J. Mater. Chem. A, 2024, 12, 4108–4122
MXene/B-Pt	14	78.6	J. Mater. Chem. A, 2023, 11, 5830–5840
$Pt_{61}Ga_{39}$ @CNT	18	25.9	Appl. Catal. B-Environ, 2023, 322, 122100
PtW NPs/C	19.4	27.8	J. Am. Chem. Soc, 2020, 142, 17250−17254
$PtCNP_2$	22	31.2	J. Mater. Chem. A, 2022, 10, 5962–5970
DC–PANI–Pt	23	36.5	J. Power Sources, 2024, 608, 234653
S-PtCo@MC	23	23	ACS Nano, 2023, 17, 3889−3900
Pt-WC/CNT	25	28.2	Small, 2024, 20, 2309675
Pt−T/G-150	26.4	30	ACS Appl. Mater. Interfaces, 2020, 12, 40204−40212
Pt@DG	30	53	J. Am. Chem. Soc, 2022, 144, 2171−2178
Pt NPs/DPC	30	31	J. Alloys Compd, 2023, 171970
Pt/A_PGnP	31	31.09	Mater. Today. Sustainability, 2023, 24, 100598
Pd_7@Pt_3	33	23.1	Mater. Horiz, 2024, 11, 1964
PtCu/WO_3@CF	41	45.9	Adv. Funct. Mater, 2022, 32, 2112207
Pt_3Co@NCNT	42	27.2	Angew. Chem. Int. Ed, 2021, 60, 19068–19073
m-Pt@MoS_2	47	32	Small, 2024, 20, 2309427

References

1 S. Wang, Q. Zhao, Q. Ma, R. Gan, Y. Ran, W. Fang, C. Wang, L. Fang, Q. Feng, Y. Zhang, D. Wang and Y. Li, *Nano Lett*, 2024, **24**, 11286-11294.

2 G. Kresse and J. Furthmüller, *Phys. Rev*. B, 1996, **54**, 11169-11186.

3 S. Grimme, J. Antony, S. Ehrlich, H. Krieg, *J. Chem. Phys*, 2010, **132**, 154104.

4 J. Li, J. Liu, C. Chen, J. Guo, R. Bi, S. Chen, L. Zhang and M. Zhu, *Chem. Eng. J*, 2022, **436**, 135186.

5 T. Zhao, M. Li, D. Xiao, X. Yang, Q. Li, L. An, Z. Deng, T. Shen, M. Gong, Y. Chen, G. Wang, X. Zhao, L. Xiao, X. Yang, L. Li and D. Wang, *J. Am. Chem. Soc*, 2023, **145**, 4088-4097.

6 L. Chen, L. Kang, S. Geng, L. Cheng, D. Cai, S. Song, H. Jia and Y. Wang, *Adv. Funct. Mater*, 2024, **34**, 2403467.

7 G. Henkelman, A. Arnaldsson and H. Jónsson, *Computational Materials Science*, 2005, **36**, 354-360.